A Model for Nonlinear Interactions of Internal Gravity Waves with Saturated Regions

Daniel Ruprecht[1*] and Rupert Klein[1]

Daniel Ruprecht:
Institut für Mathematik, Freie Universität Berlin
Arnimallee 6, 14195 Berlin, Germany
Phone: +49 30 841–85415
e-mail: ruprech@math.fu-berlin.de

Rupert Klein:
Institut für Mathematik, Freie Universität Berlin
Arnimallee 6, 14195 Berlin, Germany
Phone: +49 30 838–75414
e-mail: rupert.klein@math.fu-berlin.de

Abstract

A model for interactions between non-hydrostatic gravity waves and deep convective narrow hot towers is presented. The starting point of the derivation are the conservation laws for mass, momentum and energy for compressible flows combined with a bulk micro-physic model. Using multiscale asymptotics, a set of leading order equations is extracted, valid for the specific scales of the investigated regime. These are a timescale of 100 s, a horizontal and vertical lengthscale of 10 km for the wave dynamics plus a second horizontal lengthscale of 1 km for the narrow hot towers. Because of the comparatively short horizontal scales, Coriolis effects are negligible in this regime. The leading order equations are then closed by applying conditional averages over the hot tower lengthscale, leading to a closed model for the wave-scale that retains the net effects of the smaller scale dynamics. By assuming a systematically small saturation deficit in the ansatz, the small vertical displacements arising in this regime suffice to induce leading order changes of the saturated area fraction. The latter is the essential parameter in the model arising from the micro-physics.

Zusammenfassung

Der Artikel präsentiert ein Modell zur Beschreibung der Wechselwirkung von nichthydrostatischen Schwerewellen mit hochreichenden Konvektionswolken. Der Ausgangspunkt der Herleitung sind die Erhaltungsgleichungen für Masse, Impuls und Energie für kompressible Strömungen, kombiniert mit einem „bulk“-Modell für die Mikrophysisk. Mittels Mehrskalenasymptotik wird ein System von Gleichungen für die Dynamik führender Ordnung extrahiert, welches gerade für die spezifizierten Skalen Gültigkeit besitzt. Diese Skalen sind eine Zeitskala von 100 s, eine horizontale und vertikale Längenskala von 10 km für die Dynamik der Wellen sowie eine zweite horizontale Längenskala von 1 km für die Konvektionswolken. Aufgrund der verhältnismäßig kurzen horizontalen Längenskalen sind Coriolis-Effekte im betrachteten Regime vernachlässigbar. Das resultierende System wird durch bedingte Mittelung über die Längenskala der Konvektionswolken geschlossen und in ein Modell für die Wellenskala überführt, welches jedoch die effektiven Beiträge der kleinskaligen Dynamik beinhaltet. Im Ansatz wird ein systematisch kleines Sättigungsdefizit angenommen, so dass die im betrachteten Regime auftretenden kleinen vertikalen Auslenkungen zu Änderungen des Flächenanteils gesättigter Bereiche in führender Ordnung führen können. Dieser Flächenanteil ist der wesentliche aus der Mikrophysik abgeleitete Parameter.

1 Introduction

Interactions between internal gravity waves and moisture in the atmosphere give rise to several important effects. It is known that tropical deep moist convection generates gravity waves, see for example FOVELL et al. (1991); LANE et al. (2001), and that these waves yield a major contribution to overall wave-drag (KIM et al. (2003)). Parameterizations of this "gravity wave-drag" (see LINDZEN (1981)) are important for global circulation models to produce realistic flows. In this context, SURGI (1989) finds that using a stability frequency that includes a modification due to moisture yields improved results. On the other hand, patterns of convection are also strongly affected by gravity waves. EINAUDI and LALAS (1975); CHIMONAS et al. (1980) find that waves can trigger deep convection by helping to overcome convective inhibition. MAPES (1993) investigates mechanisms through which gravity waves contribute to the organization of convection.

Most studies investigating the interactions between gravity waves and moisture rely on the numerical solution of "full physics" models, usually the compressible or anelastic equations coupled with a bulk micro-physics model, see DURRAN and KLEMP (1983); CLARK et al. (1986); LANE et al. (2001); MIGLIETTA and ROTUNNO (2005) for example. However, because of the complexity of the involved models, it is very difficult to extract and understand the essential interaction mechanisms from the equations. For this purpose it is usually beneficial to study reduced models that describe only a certain subset of effects considered to be important while neglecting others. Because of the reduced complexity of the equations, such models are often much more accessible to mathematical analysis and can provide valuable insight into the essential dynamics of the studied subject. Approaches to study the interaction between gravity waves and moisture that feature simplified models can be found, for example, in EINAUDI and LALAS (1973), who introduce a model for gravity wave propagation in a saturated atmosphere, or in BARCILON et al. (1979, 1980); JUSEM and BARCILON (1985), who utilize a switching mechanism between a dry and a reduced moist stability frequency depending on vertical displacement. The introduction of a reduced "effective stability" by moisture is also indicated in DURRAN and KLEMP (1982).

This paper presents a reduced model for nonlinear interactions between non-hydrostatic, non-rotating gravity waves and saturated areas in an atmosphere containing deep moist convective towers. It is an extension of the linear model derived and analyzed in RUPRECHT et al. (2010). Interesting results from the analysis of the linear model are, for example, the introduction of a lower cut-off horizontal wavenumber by moisture in addition to the well-known upper cut-off as well as a reduction of the modulus of the group velocity. Both papers rely on the ansatz introduced in KLEIN and MAJDA (2006), where the conservation laws for mass, momentum, and energy of compressible flows combined with a bulk micro-physics model constitute a set of governing equations from which reduced models for specific scales are derived using multiscale asymptotics. In contrast to RUPRECHT et al. (2010), where the saturated areas constitute a passive background modulating the propagation characteristics of gravity waves, the derivation in the present paper uses a slightly modified ansatz, leading to nonlinear coupling between the saturated area fraction and the wave-scale dynamics.

The final model is introduced and explained in subsection 1.1 while details of the derivation are presented later in section 2. The present paper provides only the derivation, leaving a thorough analysis of the model's properties as well as numerical integrations for future work.

1.1 Summary of the Model

All equations below feature nondimensional quantities. Throughout this paper, superscripts indicate terms of a specific order in the employed expansion, for example $\mathbf{u}^{(0)}$ is the order unity term in the expansion of horizontal velocity.

The prognostic variables in the final model are the horizontal velocity $\mathbf{u}^{(0)}$, the wave-scale vertical velocity $\bar{w}^{(0)}$, the wave-scale potential temperature $\bar{\theta}$, the function $\pi = p^{(3)}/\rho^{(0)}$ where

$p^{(3)}$ is the pressure and $\rho^{(0)}$ the background density, the conditional averages of the tower-scale perturbations of vertical velocity and potential temperature w' and θ' and finally the local vertical displacement ξ_{us} and the area fraction of saturated regions σ. See section 2 for details on the definition of the tower-scale quantities. $\Theta_z^{(2)}$ is the moist-adiabatic background stratification.

Linearized anelastic moist dynamics:

$$
\begin{aligned}
\mathbf{u}_\tau^{(0)} + \nabla_x \pi &= 0 \\
\bar{w}_\tau^{(0)} + \pi_z &= \bar{\theta}^{(3)} \\
\bar{\theta}_\tau^{(3)} + (1-\sigma)\Theta_z^{(2)}\bar{w}^{(0)} &= \Theta_z^{(2)} w' \\
\rho^{(0)}\nabla_x \cdot \mathbf{u}^{(0)} + \left(\rho^{(0)}\bar{w}^{(0)}\right)_z &= 0
\end{aligned}
\tag{1.1}
$$

Averaged nonlinear tower-scale dynamics:

$$
\begin{aligned}
w'_\tau + \frac{\sigma_\tau}{1-\sigma} w' &= \theta' \\
\theta'_\tau + \sigma\Theta_z^{(2)} w' + \frac{\sigma_\tau}{1-\sigma}\theta' &= \sigma(1-\sigma)\Theta_z^{(2)}\bar{w}^{(0)} \\
\sigma_\tau &= \xi_{\text{us},\tau}\Psi \\
\xi_{\text{us},\tau} &= \bar{w}^{(0)} - \frac{w'}{1-\sigma}
\end{aligned}
\tag{1.2}
$$

The function Ψ characterizes the sensitivity of the saturated area fraction σ with respect to the displacement ξ_{us}. From its definition (2.36) it follows that it is always positive. Hence upward motion, that is $\xi_{\text{us},\tau} > 0$, increases the saturated area fraction while downward motion diminishes it. The wave-scale equations (1.1) are the non-hydrostatic anelastic equations, linearized around a background state with zero velocity and a stratification given by $\Theta_z^{(2)}$. However, the effective stratification in $(1.1)_3$ is $\Theta_z^{(2)}$ reduced by a factor of $(1-\sigma)$. Further, the net wave-scale dynamics result in a source term on the right hand side of $(1.1)_3$ related to release and consumption of latent heat. Note that because $\bar{w}^{(0)}$ appears on the right hand side of $(1.2)_2$ and $(1.2)_4$ there exists a bi-directional coupling between wave- and tower-scale.

If $\Psi \equiv 0$, it follows from $(1.2)_2$ that $\sigma = const$ and (1.1), (1.2) reduce to the model analyzed in Ruprecht et al. (2010).

2 Model Derivation

The derivation relies on the techniques outlined in detail in Klein (2004, 2008, 2010) and involves five steps. First, characteristic length- and time scales of the analyzed regime have to be identified. Then, corresponding coordinates resolving these scales are introduced by rescaling a set of "universal" coordinates $\mathbf{x}, z$ and t by powers of the generic asymptotic expansion parameter ε, arising from the distinguished limit introduced in Majda and Klein (2003). Expansions in powers of ε are then inserted into the governing equations, which, following Klein and Majda (2006), are the conservations laws for mass, momentum and energy for compressible flows combined with the bulk model for warm micro-physics (2.1) adopted from Grabowski (1998). Collecting all leading order equations then results in a set of equations, which finally require some form of closure in order to obtain a closed set of equations.

$$
\begin{aligned}
q_{\mathrm{v},t} + \mathbf{u}\cdot\nabla_{\|} q_{\mathrm{v}} + w q_{\mathrm{v},z} &= \\
C_{\mathrm{ev}} - C_{\mathrm{d}} & \\
q_{\mathrm{c},t} + \mathbf{u}\cdot\nabla_{\|} q_{\mathrm{c}} + w q_{\mathrm{c},z} &= \\
C_{\mathrm{d}} - C_{\mathrm{ac}} - C_{\mathrm{cr}} & \\
q_{\mathrm{r},t} + \mathbf{u}\cdot\nabla_{\|} q_{\mathrm{r}} + w q_{\mathrm{r},z} + \frac{1}{\rho}\left(\rho q_{\mathrm{r}} V_{\mathrm{T}}\right)_z &= \\
C_{\mathrm{ac}} + C_{\mathrm{cr}} - C_{\mathrm{ev}}. &
\end{aligned}
\tag{2.1}
$$

Here, q_{v}, q_{c} and q_{r} denote the nondimensional mixing ratios of vapor, cloud water, and rain water while C_{d}, C_{ev}, C_{ac}, C_{cr} represent the conversion between these species by condensation/evaporation of cloud water/vapor, evaporation of rain water, auto conversion of cloud droplets into rain, and collection of cloud water by falling rain. V_T is the terminal velocity of rain droplets.

2.1 Scales and Expansions

The derivation features a horizontal and vertical lengthscale of 10 km respectively, corresponding to the regime of non-rotating, non-hydrostatic internal waves, cf. chapter 8 in GILL (1982), as well as a second horizontal length scale of 1 km, corresponding to the order of magnitude of the diameter of deep convective hot towers indicated in LEMONE and ZIPSER (1980); STEVENS (2005). The employed time scale is 100 s, compatible with the typical value of the Brunt-Väisäla frequency of $N \sim 0.01$ s^{-1} quoted in GILL (1982). Equation (2.2) summarizes the employed scales and introduces the corresponding coordinates resolving them.

$$\begin{aligned} \text{Horizontal:} \quad & 10\ \text{km}, 1\ \text{km} \quad - \quad \mathbf{x}, \eta = \varepsilon^{-1}\mathbf{x} \\ \text{Vertical:} \quad & 10\ \text{km} \quad - \quad z \\ \text{Time:} \quad & 100\ \text{s} \quad - \quad \tau = \varepsilon^{-1} t \end{aligned} \tag{2.2}$$

The order of magnitude of vertical displacements resulting from $(2.2)_3$ and a reference velocity of 10 m s^{-1} is 1 km. Thus the nondimensional vertical displacement ξ is of the order

$$\xi \sim \frac{1\ \text{km}}{10\ \text{km}} = 0.1 = \mathcal{O}(\varepsilon). \tag{2.3}$$

Hence, as $q_{\mathrm{vs},z} = \mathcal{O}(1)$, the amount δq of released or consumed condensate by vertical displacements is also of the order

$$\delta q \sim \xi q_{\mathrm{vs},z} = \mathcal{O}(\varepsilon). \tag{2.4}$$

The saturation deficit is defined as the difference between the saturation mixing ratio q_vs and the mixing ratio of water vapor

$$\delta q_\mathrm{vs} := q_\mathrm{vs} - q_\mathrm{v}. \tag{2.5}$$

In a regime with a saturation deficit δq of order unity, condensation or evaporation of $\mathcal{O}(\varepsilon)$ amounts of vapor or cloud water cannot exert a leading order effect on the size of saturated regions, see the upper illustration in figure 1. This regime is investigated in RUPRECHT et al. (2010). There, the saturated area fraction σ is constant over time and acts as a wave-modulating background. In the present paper, a systematically small saturation deficit is assumed, that is the vapor mixing ratio q_{v} is expanded as

$$q_{\mathrm{v}}(\eta, x, z, \tau) = q_{\mathrm{vs}}^{(0)}(z) + \varepsilon q_{\mathrm{v}}^{(1)}(\eta, x, z, \tau) + \mathcal{O}(\varepsilon^2), \tag{2.6}$$

whereas $q_{\mathrm{vs}}^{(0)}$ is the leading order term of the saturation mixing ratio. From (2.6) it follows that the saturation deficit is of the order

$$\delta q_{\mathrm{vs}} = \mathcal{O}(\varepsilon), \tag{2.7}$$

so that now (2.4) suffices to induce a leading order change in the size of saturated regions, see the lower illustration in figure 1 for a sketch of this regime. The expansions of the mixing ratios of cloud water q_{c} and rain water q_{r} read

$$\begin{aligned} q_{\mathrm{c/r}}(\eta, x, z, \tau) = {} & q_{\mathrm{c/r}}^{(0)}(\eta, x, z, \tau) \\ & + \varepsilon q_{\mathrm{c/r}}^{(1)}(\eta, x, z, \tau) + \mathcal{O}(\varepsilon^2). \end{aligned} \tag{2.8}$$

The dynamical quantities are expanded as described in RUPRECHT et al. (2010), see appendix A for a summary. Note that the horizontal velocity is assumed to be independent from η at leading order.

All resulting leading order equations are split into equations for the tower-scale averages, defined by

$$\bar{\phi}(\mathbf{x}, z, \tau) := \lim_{\eta_0 \to \infty} \frac{\int_{[-\eta_0, \eta_0]^2} \phi(\eta, \mathbf{x}, z, \tau) d\eta}{\left|[-\eta_0, \eta_0]^2\right|} \tag{2.9}$$

and perturbations $\tilde{\phi} := \phi - \bar{\phi}$. Here,

$$[-\eta_0, \eta_0]^2 := \left\{(\eta_1, \eta_2) \in \mathbb{R}^2 : |\eta_1|, |\eta_2| \leq \eta_0\right\} \tag{2.10}$$

denotes the square around the origin with side lengths of $2\eta_0$. The resulting leading order equations for the averages read

$$
\begin{aligned}
\mathbf{u}_\tau^{(0)} + \nabla_x \pi &= 0 \\
\bar{w}_\tau^{(0)} + \pi_z &= \bar{\theta}^{(3)} \\
\bar{\theta}_\tau^{(3)} + \left(1 - \overline{H_{\mathrm{q_v}}}\right) \Theta_z^{(2)} \bar{w}^{(0)} &= \overline{H_{\mathrm{q_v}} \tilde{w}^{(0)}} \Theta_z^{(2)} \\
\nabla_x \cdot \left(\rho^{(0)} \mathbf{u}^{(0)}\right) + \left(\rho^{(0)} \bar{w}^{(0)}\right)_z &= 0.
\end{aligned}
\tag{2.11}
$$

The derivation of (2.11) is essentially identical to the one in RUPRECHT et al. (2010). As the present paper focusses on the modified micro-physics, the reader is referred there for details but some key-steps can be found in appendix A. The switching function in the present derivation is defined according to saturation not at leading order but at order $\mathcal{O}(\varepsilon)$, that is

$$
H_{\mathrm{q_v}} := \begin{cases} 1 : q_{\mathrm{v}}^{(1)} = q_{\mathrm{vs}}^{(1)} \\ 0 : q_{\mathrm{v}}^{(1)} < q_{\mathrm{vs}}^{(1)}. \end{cases} \tag{2.12}
$$

Note that the large-scale equations (2.11) are essentially identical to the ones in RUPRECHT et al. (2010), the difference between the two models arises due to the different effective small-scale equations derived from the micro-physical model, which determine $\overline{H_{\mathrm{q_v}} \tilde{w}^{(0)}}$ on the right hand side of $(2.11)_3$.

As the following derivations deal solely with the dynamics on the tower-scale resolved by η, the wave-scale related arguments $\mathbf{x}$ and z are omitted for the sake of a more compact notation. Unless explicitly mentioned otherwise, the occurring quantities can nevertheless depend on both wave-scale coordinates, too.

2.2 Leading Order Micro-Physics Equation

The leading order equations emerging from the micro-physics model (2.1) split into the case with saturation not only at order $\mathcal{O}(1)$ but also at order $\mathcal{O}(\varepsilon)$ and the weak under-saturated case.

Regime I (saturation):

$$
\begin{aligned}
q_v^{(1)} &= q_{\mathrm{vs}}^{(1)} \\
q_{\mathrm{c},\tau}^{(1)} + \mathbf{u}^{(0)} \cdot \nabla_\eta q_{\mathrm{c}}^{(1)} &= -w^{(0)} q_{\mathrm{vs},z}^{(0)}
\end{aligned}
\tag{2.13}
$$

Regime II (weak under-saturation):

$$
\begin{aligned}
q_{\mathrm{v},\tau}^{(1)} + \mathbf{u}^{(0)} \cdot \nabla_\eta q_{\mathrm{v}}^{(1)} &= -w^{(0)} q_{\mathrm{vs},z}^{(0)} \\
q_{\mathrm{c},\tau}^{(1)} + \mathbf{u}^{(0)} \cdot \nabla_\eta q_{\mathrm{c}}^{(1)} &= 0
\end{aligned}
\tag{2.14}
$$

The derivation exploits that $q_{\mathrm{vs}}^{(0)}$, $q_{\mathrm{vs}}^{(1)}$ both depend on z only, cf. Klein and Majda (2006), and assumes $q_{\mathrm{c}}^{(0)} = q_{\mathrm{r}}^{(0)} = 0$ at $\tau = 0$. Because of this assumption and $\delta q_{\mathrm{vs}}^{(0)} = 0$, the terms $C_{\mathrm{ev}}^{(0)}$ and $C_{\mathrm{cr}}^{(0)}$ arising in Ruprecht et al. (2010) and describing evaporation of rain water and collection of cloud water by falling rain vanish and do not occur here. Introduce the material derivative

$$
D_\tau = \partial_\tau + \mathbf{u}^{(0)} \cdot \nabla_\eta, \tag{2.15}
$$

the leading order vertical displacement $\xi^{(0)}$ defined as the solution of

$$
D_\tau \xi^{(0)} = w^{(0)} = \bar{w}^{(0)} + \tilde{w}^{(0)} \tag{2.16}
$$

and the first order total water mixing ratio

$$
q_{\mathrm{T}} := q_{\mathrm{vs}}^{(0)} + \varepsilon \left(q_{\mathrm{v}}^{(1)} + q_{\mathrm{c}}^{(1)} \right). \tag{2.17}
$$

Letting

$$
q_{\mathrm{T},0}(\eta) := q_{\mathrm{T}}(\eta, 0) \tag{2.18}
$$

denote some prescribed initial distribution of q_{T}, combining (2.13) and (2.14) and integrating in time yields

$$
q_{\mathrm{T}}(\eta, \tau) = q_{\mathrm{T},0}(\eta - \int_0^\tau \mathbf{u}^{(0)} d\tau') - \varepsilon q_{\mathrm{vs},z}^{(0)} \xi^{(0)}(\eta, \tau), \tag{2.19}
$$

exploiting that $\mathbf{u}^{(0)}$ does not depend on η and using (2.16). Thus, for the employed scaling, the leading order vapor mixing ratio $q_{\mathrm{vs}}^{(0)}$ in a rising parcel acts as an "infinite" reservoir from which, in regime I, $\mathcal{O}(\varepsilon)$ amounts of vapor condensate into cloud water $q_{\mathrm{c}}^{(1)}$ or, in regime II, are deposited into $q_{\mathrm{v}}^{(1)}$. Once $q_{\mathrm{v}}^{(1)}$ reaches the saturation threshold $q_{\mathrm{vs}}^{(1)}$, the regime switches from II to I and further ascend starts generating $q_{\mathrm{c}}^{(1)}$. Vice versa, in a descending parcel, $q_{\mathrm{v}}^{(1)}$ and $q_{\mathrm{c}}^{(1)}$ respectively are deposited back into $q_{\mathrm{vs}}^{(0)}$. In this case, at first the cloud water evaporates and once $q_{\mathrm{c}}^{(1)}$ is depleted, the regime switches from I to II and $q_{\mathrm{v}}^{(1)}$ starts to decrease.

The equations for the perturbations $\tilde{w}^{(0)}$, $\tilde{\theta}^{(3)}$ obtained by subtracting (2.11) from (A10) read

$$
\begin{aligned}
\tilde{w}_{\tau}^{(0)} + \nabla_{\eta} \cdot \left(\mathbf{u}^{(0)} \tilde{w}^{(0)}\right) &= \tilde{\theta}^{(3)} \\
\tilde{\theta}_{\tau}^{(3)} + \nabla_{\eta} \cdot \left(\mathbf{u}^{(0)} \tilde{\theta}^{(3)}\right) + \tilde{w}^{(0)} \Theta_{z}^{(2)} &= \\
H_{\mathrm{q_v}} \left(\bar{w}^{(0)} + \tilde{w}^{(0)}\right) \Theta_{z}^{(2)} & \\
-\overline{H_{\mathrm{q_v}} \left(\bar{w}^{(0)} + \tilde{w}^{(0)}\right)} \Theta_{z}^{(2)}, &
\end{aligned}
\tag{2.20}
$$

utilizing that $\mathbf{u}^{(0)}$ by assumption independent of η.

2.3 Displacement in Regime II

In regime I where $H_{\mathrm{q_v}} = 1$, (2.20)$_2$ becomes

$$
\begin{aligned}
\tilde{\theta}_{\tau}^{(3)} + \nabla_{\eta} \cdot \left(\mathbf{u}^{(0)} \tilde{\theta}^{(0)}\right) &= \\
\bar{w}^{(0)} \Theta_{z}^{(2)} - \overline{H_{\mathrm{q_v}} \left(\bar{w}^{(0)} + \tilde{w}^{(0)}\right)} \Theta_{z}^{(2)}, &
\end{aligned}
\tag{2.21}
$$

while in regime II, that is for $H_{\mathrm{q_v}} = 0$, it reads

$$
\begin{aligned}
\tilde{\theta}_{\tau}^{(3)} + \nabla_{\eta} \cdot \left(\mathbf{u}^{(0)} \tilde{\theta}^{(0)}\right) + \tilde{w}^{(0)} \Theta_{z}^{(2)} &= \\
-\overline{H_{\mathrm{q_v}} \left(\bar{w}^{(0)} + \tilde{w}^{(0)}\right)} \Theta_{z}^{(2)}. &
\end{aligned}
\tag{2.22}
$$

Thus, $\tilde{w}^{(0)}$ and $\tilde{\theta}^{(3)}$ evolve purely due to large-scale forcing in regime I but oscillate with frequency $\sqrt{\Theta_{z}^{(2)}}$ in regime II. Assuming that $\tilde{w}^{(0)}$ and $\tilde{\theta}^{(3)}$ are initially constant on the η-scale in regime II, then at $\tau > 0$ they are constant in all areas that never belonged to regime I up to this time as identical oscillations with frequency $\sqrt{\Theta_z^{(2)}}$ are performed at every point. Hence

$$\begin{aligned} &\nabla_\eta \tilde{w}^{(0)}(\eta,\tau) = \nabla_\eta \tilde{\theta}^{(3)}(\eta,\tau) = 0 \\ &\qquad \text{if } H_{\mathrm{q_v}}(\eta,\tau') = 0 \,\forall \tau' \leq \tau. \end{aligned} \tag{2.23}$$

Note that $\sqrt{\Theta_z^{(2)}}$ is the maximum frequency of waves in the large scale system (2.11), so (2.20) describes small-scale and high frequency oscillations. If at some point η the regime switches from I to II, $\tilde{w}^{(0)}$ and $\tilde{\theta}^{(3)}$ start oscillating with initial values equal to the final values in the regime I dynamics. As the interface between regime I and II moves, spatial variations in $\tilde{w}^{(0)}$, $\tilde{\theta}^{(3)}$ are generated in formerly saturated regions that become under-saturated, even for constant initial values. Now the ad-hoc assumption is made that these small-scale, high frequency oscillations can be neglected, that is

$$\tilde{w}^{(0)}(\eta,\tau) \equiv \tilde{w}_{\mathrm{us}}(\tau),\ \tilde{\theta}^{(3)}(\eta,\tau) \equiv \tilde{\theta}_{\mathrm{us}}(\tau) \tag{2.24}$$

in regime II, whereas $\tilde{w}_{\mathrm{us}}$, $\tilde{\theta}_{\mathrm{us}}$ are the constant values in all the time under-saturated areas. See figure 2 for a sketch. This approximation is motivated not by meteorological considerations but rather by the resulting mathematical simplifications, see (2.35), that allow to close the model by analytical means. An improved representation presumably still allowing for an analytically computed closure could, for example, attempt to capture the excited oscillation by adding a term $A_{1/2}\exp(i\sqrt{\Theta^{(2}}_z\tau)$ to $\tilde{w}_{\mathrm{us}}$ and $\tilde{\theta}_{\mathrm{us}}$ in (2.24), where $A_{1/2}$ are determined by the time of the regime switch. Further, the comparatively simple structure of (2.21) and (2.22) might even allow to employ analytical solutions in the closure. The present derivation, however, utilizes the simple approximation (2.24) and improvements of the representation of the $\tilde{w}^{(0)}$ and $\tilde{\theta}^{(3)}$ in under-saturated regions are left for future work. Note that, aside from the adopted asymptotic limit, (2.24) is the only ad-hoc assumption used in the derivation.

Define the displacement in under-saturated areas ξ_{us} by replacing $\tilde{w}^{(0)}$ by $\tilde{w}_{\mathrm{us}}$ in (2.16), that is

$$D_\tau \xi_{\rm us}(\tau) = \partial_\tau \xi_{\rm us}(\tau) = \bar{w}^{(0)}(\tau) + \tilde{w}_{\rm us}(\tau). \tag{2.25}$$

Introduce the function

$$q_*(\eta,\tau) := \varepsilon^{-1}\left[q_{\rm T}(\eta,\tau) - \left(q_{\rm vs}^{(0)} + \varepsilon q_{\rm vs}^{(1)}\right)\right]. \tag{2.26}$$

The initial distribution $q_{\rm T,0}$ prescribes the initial distribution of q_* via

$$q_{*,0} := q_*(\eta,0) = \varepsilon^{-1}\left[q_{\rm T,0}(\eta) - \left(q_{\rm vs}^{(0)} + \varepsilon q_{\rm vs}^{(1)}\right)\right]. \tag{2.27}$$

It follows from (2.17) that

$$q_* = \begin{cases} q_{\rm c}^{(1)} & : H_{\rm q_v} = 1 \\ q_{\rm v}^{(1)} - q_{\rm vs}^{(1)} & : H_{\rm q_v} = 0, \end{cases} \tag{2.28}$$

hence q_* is positive in regime I and negative in regime II. As $q_{\rm vs}^{(0)}$, $q_{\rm vs}^{(1)}$ depend on z only, it follows from (2.19) that when employing approximation (2.24), q_* is given by

$$q_*(\eta,\tau) = q_{*,0}(\eta - \int_0^\tau \mathbf{u}^{(0)} d\tau') - q_{{\rm vs},z}^{(0)} \xi_{\rm us}(\tau). \tag{2.29}$$

Further, we have

$$\nabla_\eta q_*(\eta,\tau) = \nabla_\eta q_{*,0}(\eta - \int_0^\tau \mathbf{u}^{(0)} d\tau'), \tag{2.30}$$

hence the shape of q_* is not altered. It is horizontally advected by $\mathbf{u}^{(0)}$ and increased or reduced by η-independent values $q_{{\rm vs},z}^{(0)}\xi_{\rm us}$, see figure 3. In order to close the model, we employ q_* as a level set function approximately tracking saturated and non-saturated regions. This is outlined in subsection 2.4.

2.4 Closing the Model

Denote by A_i an individual saturated spot, that is a connected set of points in the η-plane for which q_* is positive in the interior and zero at the boundary. Further, denote the boundary by ∂A_i, the velocity at which ∂A_i is moving by $\mathbf{v}_i$ and finally the outward pointing normal vector on ∂A_i by $\mathbf{n}$, see figure 4. Then the evolution equation for the level set function tracking the boundary, cf. WILLIAMS (1985); OSHER and FEDKIW (2002), reads

$$\partial_\tau q_* + \mathbf{v}_i \cdot \nabla_\eta q_* = 0. \tag{2.31}$$

Using (2.29) it follows that

$$\left(\mathbf{u}^{(0)} - \mathbf{v}_i\right) \cdot \nabla_\eta q_* = -q^{(0)}_{\mathrm{vs},z} \left(\bar{w}^{(0)} + \tilde{w}_{\mathrm{us}}\right). \tag{2.32}$$

Note that because ∂A_i is a contour line of q_* and q_* is positive inside A_i and negative outside, $\mathbf{n}$ points in the opposite direction as $\nabla_\eta q_*$, hence

$$\mathbf{n} = -\frac{\nabla_\eta q_*}{|\nabla_\eta q_*|}. \tag{2.33}$$

By employing (2.30) and (2.33), (2.32) becomes

$$\mathbf{v}_i \cdot \mathbf{n} = \mathbf{u}^{(0)} \cdot \mathbf{n} - q^{(0)}_{\mathrm{vs},z} \frac{\bar{w}^{(0)} + \tilde{w}_{\mathrm{us}}}{\left|\nabla_\eta q_{*,0}(\eta - \int_0^\tau \mathbf{u}^{(0)} d\tau')\right|}. \tag{2.34}$$

The boundary ∂A_i is characterized by the condition

$$q_*(\eta, \tau) = 0 \Leftrightarrow q_{*,0}(\eta - \int_0^\tau \mathbf{u}^{(0)} d\tau') = q^{(0)}_{\mathrm{vs},z} \xi_{\mathrm{us}}(\tau), \tag{2.35}$$

cf. (2.29), and is thus fully determined by the displacement and the initial distribution $q_{*,0}$. This is the important simplification obtained by introducing approximation (2.24). For given $q_{*,0}$, define

$$\begin{aligned} \Psi_i(\xi_{\mathrm{us}}, \tau) &:= \oint_{\partial A_i} \mathbf{v}_i \cdot \mathbf{n} dS \\ &= -q^{(0)}_{\mathrm{vs},z} \oint_{\partial A_i} \frac{1}{\left|\nabla_\eta q_{*,0}(\eta - \int_0^\tau \mathbf{u}^{(0)} d\tau')\right|} dS, \end{aligned} \tag{2.36}$$

using (2.34) and that $\mathbf{u}^{(0)}$ is independent of η, hence the surface integral over $\mathbf{u}^{(0)} \cdot \mathbf{n}$ vanishes. Note that for a fixed value of ξ_{us}, it is $\Psi_i(\xi_{\mathrm{us}}, \tau) = \Psi_i(\xi_{\mathrm{us}}, 0)$, because the saturated spot A_i as well as q_* are simply advected horizontally with $\mathbf{u}^{(0)}$. The function Ψ_i determines how sensitive the size of the saturated spot depends on the displacement ξ_{us}. Steep gradients of q_* lead to a weak sensitivity while small gradients result in a strong dependence of $|A_i|$ on $\xi_{\rm us}$, cf. figure 3. In the limit $|\nabla_\eta q_*| \to \infty$, the coupling vanishes and the linear model from RUPRECHT et al. (2010) is retrieved. Note that the saturation mixing ratio decreases with height, hence $q^{(0)}_{{\rm vs},z} < 0$, so that

$$\Psi_i(\xi_{\rm us}, \tau) \geq 0 \tag{2.37}$$

holds for any value of $\xi_{\rm us}$ or τ as well as any initial distribution $q_{*,0}$.

By integrating (2.20) over a saturated spot A_i moving at velocity $\mathbf{v}_i$, the following balances are obtained

$$\begin{aligned}
&\frac{\partial}{\partial\tau}\int_{A_i}\tilde{w}d\eta + \oint_{\partial A_i}\tilde{w}\left(\mathbf{u}^{(0)} - \mathbf{v}_i\right)\cdot\mathbf{n}dS = \int_{A_i}\tilde{\theta}d\eta\\
&\frac{\partial}{\partial\tau}\int_{A_i}\tilde{\theta}d\eta + \oint_{\partial A_i}\tilde{\theta}\left(\mathbf{u}^{(0)} - \mathbf{v}_i\right)\cdot\mathbf{n}dS + \Theta_z^{(2)}\int_{A_i}\tilde{w}d\eta\\
&= \Theta_z^{(2)}\bar{w}^{(0)}\int_{A_i}\left(H_{\rm q_v} - \overline{H}_{\rm q_v}\right)d\eta\\
&+ \Theta_z^{(2)}\int_{A_i}\left(H_{\rm q_v}\tilde{w}^{(0)} - \overline{H_{\rm q_v}\tilde{w}^{(0)}}\right)d\eta.
\end{aligned} \tag{2.38}$$

see for example THOMAS and LOMBARD (1979). Now, using (2.24) and (2.34) yields

$$\begin{aligned}
&\partial_\tau\int_{A_i}\tilde{w}^{(0)}d\eta - \tilde{w}_{\rm us}\left(\bar{w}^{(0)} + \tilde{w}_{\rm us}\right)\Psi_i = \int_{A_i}\tilde{\theta}^{(3)}\\
&\partial_\tau\int_{A_i}\tilde{\theta}^{(3)}d\eta - \tilde{\theta}_{\rm us}\left(\bar{w}^{(0)} + \tilde{w}_{\rm us}\right)\Psi_i + \Theta_z^{(2)}\int_{A_i}\tilde{w}^{(0)}d\eta\\
&= \Theta_z^{(2)}\bar{w}^{(0)}\int_{A_i}\left(H_{\rm q_v} - \overline{H}_{\rm q_v}\right)d\eta\\
&+ \Theta_z^{(2)}\int_{A_i}\left(H_{\rm q_v}\tilde{w}^{(0)} - \overline{H_{\rm q_v}\tilde{w}^{(0)}}\right)d\eta,
\end{aligned} \tag{2.39}$$

exploiting again that $\mathbf{u}^{(0)}$ is independent from η. Let $D(\eta_0) = [-\eta_0, \eta_0]^2$ denote a square containing a finite number of saturated spots $A_1, \ldots, A_{n(\eta_0)}$, cf. figure 5. Introduce the weighted averages

$$
\begin{aligned}
w' &:= \overline{H_{\mathrm{q_v}}\tilde{w}^{(0)}} \\
\theta' &:= \overline{H_{\mathrm{q_v}}\tilde{\theta}^{(3)}} \\
\sigma &:= \overline{H}_{\mathrm{q_v}} \\
\Psi &:= \lim_{\eta_0\to\infty} \frac{\sum_{i=1}^{n(\eta_0)} \Psi_i}{\int_{D(\eta_0)} \mathbf{1} d\eta}.
\end{aligned}
\tag{2.40}
$$

Note that because the spots A_i are advected with $\mathbf{u}^{(0)}$, the choice of spots located in a finite square $D(\eta_0)$ changes with time. Hence the series in (2.40)$_4$ is rearranged depending on τ. Assuming that it converges absolutely, however, for a given ξ_{us}, the limit Ψ of every rearrangement is the same and thus independent of time. Because according to (2.37) all terms of the series are positive, absolute convergence immediately follows from convergence. Sum up the balances (2.39), use that $H_{\mathrm{q_v}}$ is the characteristic function of the union of all A_i, hence

$$
\sum_{i=1}^{n(\eta_0)} \int_{A_i} f d\eta = \int_{D(\eta_0)} H_{\mathrm{q_v}} f d\eta \tag{2.41}
$$

for any function f, and then apply the limit $\eta_0 \to \infty$ to obtain

$$
\begin{aligned}
& w'_\tau - \tilde{w}_{\mathrm{us}} \left(\bar{w}^{(0)} + \tilde{w}_{\mathrm{us}} \right) \Psi = \theta' \\
& \theta'_\tau - \tilde{\theta}_{\mathrm{us}} \left(\bar{w}^{(0)} + \tilde{w}_{\mathrm{us}} \right) \Psi + \sigma \Theta_z^{(2)} w' \\
& = \sigma(1-\sigma)\Theta_z^{(2)} \bar{w}^{(0)}.
\end{aligned}
\tag{2.42}
$$

An expression for the evolution of σ can be derived from (2.34) in a similar way, employing (2.41) with $f \equiv 1$ to get

$$
\partial_\tau \sigma = \left(\bar{w}^{(0)} + \tilde{w}_{\mathrm{us}} \right) \Psi. \tag{2.43}
$$

Finally, the constant velocity $\tilde{w}_{\mathrm{us}}$ can be computed from w' via

$$
\begin{aligned}
\tilde{w}_{\mathrm{us}} &= \lim_{\eta_0\to\infty} \frac{\int_{D(\eta_0)} (1 - H_{\mathrm{q_v}})\, \tilde{w}^{(0)}\, d\eta}{\int_{D(\eta_0)} (1 - H_{\mathrm{q_v}})\, d\eta} \\
&= \left(\bar{\tilde{w}}^{(0)} - w'\right) \frac{1}{1-\sigma} \\
&= -w' \frac{1}{1-\sigma}.
\end{aligned}
\tag{2.44}
$$

The final model, consisting of (1.1) and (1.2), is obtained by combining (2.25), (2.42) and (2.43) with (2.44).

3 Summary

This paper presents a reduced model for interactions of non-hydrostatic, non-rotating gravity waves with saturated areas in tropical deep convective clouds. The derivation features two horizontal lengthscales, one related to the wave-dynamics and one related to the typical diameter of the hot towers. The conservation laws for mass, momentum and energy for compressible flows together with a bulk micro-physics model for vapor, cloud water and rain water mixing ratios are employed as governing equations. From these, using multiscale asymptotics, a set of leading order equations for the specific length- and timescales of the investigated regime is devised. This set of leading order equations is then turned into a closed model for the wave-scale dynamics by applying conditional averages over the tower-scale, eliminating the explicit dependence on the small scale coordinate while retaining the net effects of the micro-physics on the larger scale. A level-set approach is employed in the closure to track the growing and shrinking saturated regions. The essential moisture-related parameter in the final model is the saturated area fraction in horizontal slices on the lengthscale of the convective clouds. It evolves according to the vertical displacement generated by the wave-scale and net micro-scale vertical velocity. However, one ad-hoc approximation is introduced in the closure procedure at this stage: Tower-scale gradients of vertical velocity and potential temperature are neglected that arise in areas becoming saturated and under-saturated again. The scope of this paper is the derivation of the model and a detailed analysis is left for future work.

Acknowledgments

The authors thank Andrew J. Majda for helpful discussions. This work is funded by the DFG Priority Research Program "PQP" (SSP 1167 Quantitative Precipitation Forecast) and by the Leibniz-Gemeinschaft (WGL) through the PAKT project "High-resolution Modelling of Clouds and Gravity Waves".

A Key-Steps in Derivation

This appendix briefly repeats the essential intermediate steps arising in the derivation of the equations for the dynamical quantities. First, the governing non-dimensional equations are quoted, then the employed asymptotic expansions of the dynamical quantities are presented and finally the leading order dynamical equations are given. Additional details on the governing equations, the expansions and the key-steps can be found in KLEIN and MAJDA (2006); RUPRECHT et al. (2010); RUPRECHT (2010).

A.1 Nondimensional Governing Equations

The non-dimensional conservation laws for mass, momentum, energy (expressed as potential temperature), quoting from KLEIN and MAJDA (2006), read

$$
\begin{aligned}
&\rho_t + \nabla_{||} \cdot (\rho \mathbf{u}) + (\rho w)_z = 0 \\
&\mathbf{u}_t + \mathbf{u} \cdot \nabla_{||} \mathbf{u} + w \mathbf{u}_z + \epsilon f \left(\Omega \times \mathbf{v} \right)_{||} + \epsilon^{-4} \rho^{-1} \nabla_{||} p = 0 \\
&w_t + \mathbf{u} \cdot \nabla_{||} w + w w_z + \epsilon f \left(\Omega \times \mathbf{v} \right)_{\perp} + \epsilon^{-4} \rho^{-1} p_z = -\epsilon^{-4} \\
&\theta_t + \mathbf{u} \cdot \nabla_{||} \theta + w \theta_z = \quad \epsilon^2 \left(\tilde{S}_\theta^\epsilon + S_\theta^{q,\epsilon} \right)
\end{aligned}
\tag{A1}
$$

where

$$S_{\theta}^{q,\epsilon} = \Gamma^{**} L^{**} q_{\mathrm{vs}}^{**} \frac{\theta}{p} \left(\epsilon^{-n} \hat{C}_{\mathrm{d}} - \hat{C}_{\mathrm{ev}} \right) \tag{A2}$$

is the source term related to evaporation and condensation, while $\tilde{S}_{\theta}^{\epsilon}$ is a given external source of energy like, for example, radiation. The latter is set to zero in the present derivation. Note that as the derivation features two horizontal coordinates, the gradient transforms like

$$\nabla_{||} \mapsto \nabla_{\mathbf{x}} + \varepsilon^{-1} \nabla_{\eta}. \tag{A3}$$

A.2 Asymptotic Expansions

The vertical velocity is expanded as

$$w(\mathbf{x}, z, t; \varepsilon) = w^{(0)}(\eta, \mathbf{x}, z, \tau) + \mathcal{O}(\varepsilon), \tag{A4}$$

while the horizontal velocity is assumed to be independent from the micro-scale coordinate at leading order and therefore expanded as

$$u(\mathbf{x}, z, t; \varepsilon) = \mathbf{u}^{(0)}(\mathbf{x}, z, \tau) + \mathcal{O}(\varepsilon). \tag{A5}$$

The potential temperature is expanded around a background stratification $\overline{\theta}(z) = 1 + \epsilon^2 \Theta^{(2)}(z)$ as

$$\begin{aligned} \theta(\mathbf{x}, z, t; \varepsilon) = 1 + \varepsilon^2 \Theta^{(2)}(z) \\ + \varepsilon^3 \theta^{(3)}(\eta, \mathbf{x}, z, \tau) + \mathcal{O}(\varepsilon^4). \end{aligned} \tag{A6}$$

Finally, pressure and density are expanded as

$$\begin{aligned} (p, \rho)(\mathbf{x}, z, t; \varepsilon) &= (p^{(0)}, \rho^{(0)})(z) + \varepsilon (p^{(1)}, \rho^{(1)})(z) \\ &+ \varepsilon^2 (p^{(2)}, \rho^{(2)})(z) \\ &+ \varepsilon^3 (p^{(3)}, \rho^{(3)})(\eta, \mathbf{x}, z, \tau) + \mathcal{O}(\varepsilon^4). \end{aligned} \tag{A7}$$

A.3 Leading Order Equations

After a few transformations employing the key equations, cf. the appendix in Ruprecht et al. (2010),

$$\nabla_\eta p^{(3)} = 0 \tag{A8}$$

and

$$\hat{L} H_{\mathrm{q_v}} C_{\mathrm{d}}^{(0)} = H_{\mathrm{q_v}} \left(\bar{w}^{(0)} + \tilde{w}^{(0)} \right) \Theta_z^{(2)}, \tag{A9}$$

whereas $\hat{L}$ incorporates a number of $\mathcal{O}(1)$ constants arising during the non-dimensionalization, the leading order equations for the dynamic quantities $\mathbf{u}$, w, θ, p and ρ read

$$\begin{aligned}
&\mathbf{u}_\tau^{(0)} + \nabla_x \pi + \nabla_\eta \left(p^{(4)} / \rho^{(0)} \right) = 0 \\
&w_\tau^{(0)} + \mathbf{u}^{(0)} \cdot \nabla_\eta w^{(0)} + \pi_z = \theta^{(3)} \\
&\rho^{(0)} \nabla_\eta \cdot \mathbf{u}^{(1)} + \rho^{(0)} \nabla_x \cdot \mathbf{u}^{(0)} + \left(\rho^{(0)} w^{(0)} \right)_z = 0 \\
&\theta_\tau^{(3)} + \mathbf{u}^{(0)} \cdot \nabla_\eta \theta^{(3)} + w^{(0)} \Theta_z^{(2)} \\
&\quad = H_{\mathrm{q_v}} \left(\bar{w}^{(0)} + \tilde{w}^{(0)} \right) \Theta_z^{(2)}.
\end{aligned} \tag{A10}$$

Note that the term $C_{\mathrm{ev}}^{(0)}$ occurring in Ruprecht et al. (2010), describing cooling by evaporation rain water, vanishes here because saturation at leading order is assumed. The η-gradient of $p^{(4)}$ and the η-divergence of $\mathbf{u}^{(1)}$ vanish by applying a sublinear growth condition. Averaging over η then yields (1.1).

References

Barcilon, A., J. C. Jusem, P. G. Drazin, 1979: On the two-dimensional, hydrostatic flow of a stream of moist air over a mountain ridge. – Geophys. Astrophys. Fluid Dynamics **13**, 125–140.

Barcilon, A., J. C. Jusem, S. Blumsack, 1980: Pseudo-adiabatic flow over a two-dimensional ridge. – Geophys. Astrophys. Fluid Dynamics **16**, 19–33.

Chimonas, G., F. Einaudi, D. P. Lalas, 1980: A wave theory for the onset and initial growth of condensation in the atmosphere. – J. Atmos. Sci. **37**, 827–845.

Clark, T. L., T. Hauf, J. P. Kuettner, 1986: Convectively forced internal gravity waves: Results from two-dimensional numerical experiments. – Quart. J. R. Met. Soc. **112**, 899–925.

Durran, D. R., J. B. Klemp, 1982: On the effects of moisture on the Brunt-Väisälä frequency. – J. Atmos. Sci. **39**, 2152–2158.

Durran, D. R., J. B. Klemp, 1983: A compressible model for the simulation of moist mountain waves. – Mon. Wea. Rev. **111**, 2341–2361.

Einaudi, F., D. P. Lalas, 1973: The propagation of acoustic-gravity waves in a moist atmosphere. – J. Atmos. Sci. **30**, 365–376.

Einaudi, F., D. P. Lalas, 1975: Wave-induced instabilites in an atmosphere near saturation. – J. Atmos. Sci. **32**, 536–547.

Fovell, R., D. Durran, J. R. Holton, 1991: Numerical simulation of convectively generated stratospheric gravity waves. – J. Atmos. Sci. **49**, 1427–1442.

Gill, A. E., 1982: Atmosphere-Ocean Dynamics – Academic Press, 662.

Grabowski, W. W., 1998: Toward cloud resolving modeling of large-scale tropical circulations: A simple cloud microphysics parameterization. – J. Atmos. Sci. **55**, 3283–3298.

Jusem, J. C., A. Barcilon, 1985: Simulation of moist mountain waves with an anelastic model. – Geophys. Astrophys. Fluid Dynamics **33**, 259–276.

KIM, Y.-J., S. D. ECKERMANN, H.-Y. CHUN, 2003: An overview of the past, present and future of gravity-wave drag parameterization for numerical climate and weather prediction models. – Atmosphere-Ocean **41**(1), 65–98.

KLEIN, R., 2004: An applied mathematical view of meteorological modelling. – In: Applied Mathematics Entering the 21st century; Invited talks from the ICIAM 2003 Congress, volume 116. SIAM Proceedings in Applied Mathematics.

KLEIN, R., 2008: An unified approach to meteorological modelling based on multiple-scales asymptotics. – Adv. Geosci. **15**, 23–33.

KLEIN, R., 2010: Scale-dependent models for atmospheric flows. – Annu. Rev. Fluid Mech. **42**, 249–274.

KLEIN, R., A. MAJDA, 2006: Systematic multiscale models for deep convection on mesoscales. – Theor. & Comput. Fluid Dyn. **20**, 525–551.

LANE, T. P., M. J. REEDER, T. L. CLARK, 2001: Numerical modeling of gravity wave generation by deep tropical convection. – J. Atmos. Sci. **58**, 1249–1274.

LEMONE, M. A., E. J. ZIPSER, 1980: Cumulonimbus vertical velocity events in GATE. Part I: Diameter, intensity and mass flux. – J. Atmos. Sci. **37**, 2444–2457.

LINDZEN, R. S., 1981: Turbulence and stress owing to gravity wave and tidal breakdown. – J. Geophys. Res. **86**, 9707–9714.

MAJDA, A., R. KLEIN, 2003: Systematic multi-scale models for the tropics. – J. Atmos. Sci. **60**, 393–408.

MAPES, B. E., 1993: Gregarious tropical convection. – J. Atmos. Sci. **50**, 2026–2037.

MIGLIETTA, M. M., R. ROTUNNO, 2005: Simulations of moist nearly neutral flow over a ridge. – J. Atmos. Sci. **62**, 1410–1427.

OSHER, S., R. FEDKIW, 2002: Level Set Methods and Dynamic Implicit Surfaces – Springer, 296.

RUPRECHT, D., 2010: Analysis of a multi-scale asymptotic model for internal gravity waves in a moist atmosphere Ph.D. thesis, Freie Universität Berlin.

RUPRECHT, D., R. KLEIN, A. J. MAJDA, 2010: Modulation of internal gravity waves in a multi-scale model for deep convection on mesoscales. – J. Atmos. Sci. , In press.

STEVENS, B., 2005: Atmospheric moist convection. – Annu. Rev. Earth. Planet. Sci. **33**, 605–643.

SURGI, N., 1989: Systematic errors of the FSU global spectral model. – Mon. Wea. Rev. **117**, 1751–1766.

THOMAS, P. D., C. K. LOMBARD, 1979: Geometric conservation law and its application to flow computations on moving grids. – AIAA Journal **17**(10), 1030–1037.

WILLIAMS, F., 1985: Turbulent combustion. – In: J. BUCKMASTER (Ed.), The Mathematics of Combustion, 97–131, Philadelphia. SIAM.

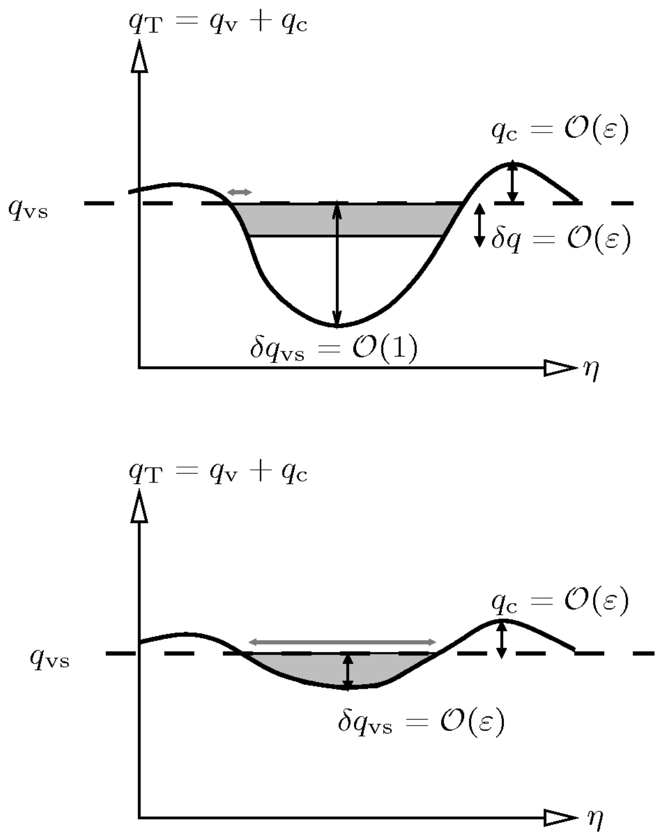

Figure 1: *Example distribution of total water $q_{\mathrm{T}} = q_{\mathrm{v}} + q_{\mathrm{c}}$, that is the sum of vapor and cloud water mixing ratio (thick solid line). The grey areas indicate the $\mathcal{O}(\varepsilon)$ amount of condensate released by the small vertical displacements allowed for by the employed short time scale, cf.* (2.4)*. The dashed horizontal line denotes the saturation mixing ratio. For a saturation deficit δq_{vs} at leading order* (upper)*, there is only a small change in the size of the saturated area (indicated by grey double arrows), while the change is of order unity in the case of a systematically small saturation deficit* (lower)*. In both cases, the mixing ratio of cloud water in saturated areas, that is the difference $q_{\mathrm{T}} - q_{\mathrm{vs}}$, is small and of order $\mathcal{O}(\varepsilon)$.*

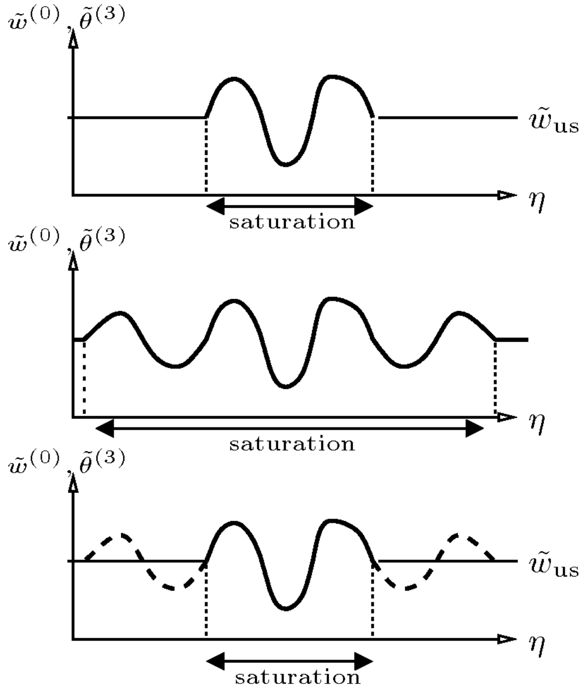

Figure 2: *General structure of the perturbation vertical velocity $\tilde{w}^{(0)}$ and potential temperature $\tilde{\theta}^{(3)}$ on the η-coordinate. Initially, variations are present only in the saturated area, i.e. in regime I* (upper). *As the saturated area enlarges, variations can arise in the now saturated areas* (middle). *As the saturated region shrinks again, variations in the again under-saturated areas (dashed line) are neglected and the constant value $\tilde{w}_{\mathrm{us}}$ or $\tilde{\theta}_{\mathrm{us}}$ is employed* (lower).

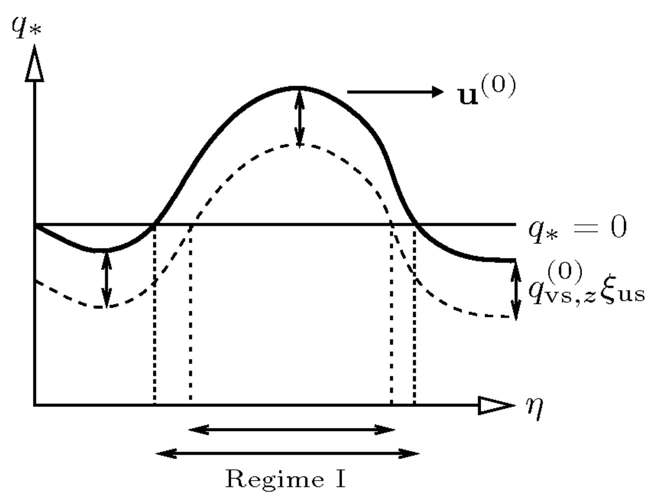

Figure 3: *The level set function q_* tracking the interface between regime I (saturation) and II (weak under-saturation). Its gradient remains constant in time, while q_* is moved upward (if $\xi_{\mathrm{us}} > 0$) or downward (if $\xi_{\mathrm{us}} < 0$) as well as horizontally advected by $\mathbf{u}^{(0)}$. Regime I is identified with regions where $q_* > 0$ while regime II is identified with areas where $q_* < 0$. However, because of* (2.24)*, this involves some degree of approximation. Note that steeper gradients of q_* lead to a less sensitive dependence of the size of saturated regions on displacement.*

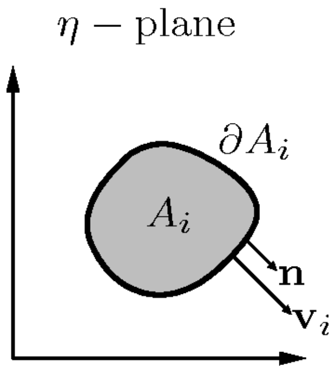

Figure 4: *Example of a saturated patch A_i in the η-plane. It is $q_* > 0$ inside A_i, $q_* = 0$ on its boundary denoted by ∂A_i and $q_* < 0$ outside of A_i. The outward directed normal vector on the boundary is denoted by $\mathbf{n}$ and the velocity at which the boundary is moving by $\mathbf{v}_i$. Note that at every fixed point on ∂A_i, $\mathbf{n}$ and $\mathbf{v}_i$ are collinear, but while $\mathbf{n}$ always points out of A_i, $\mathbf{v}_i$ can also point into the patch, for example if the patch is shrinking.*

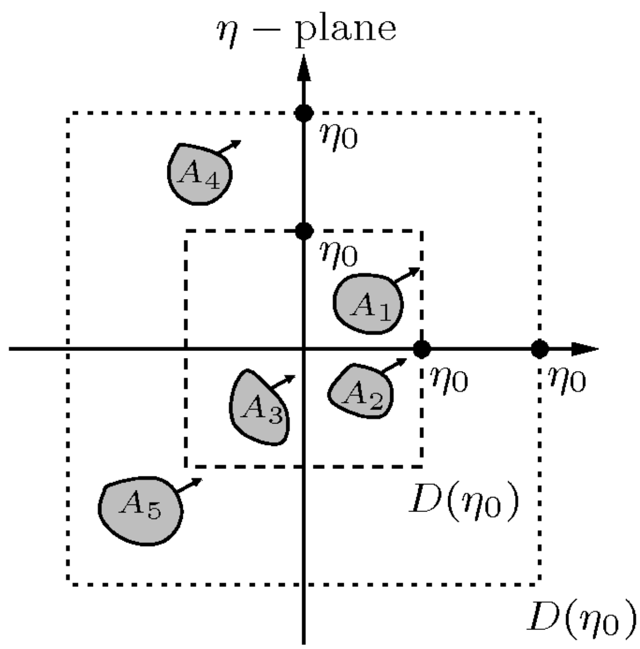

Figure 5: *Visualization of $D(\eta_0)$ for two different values of η_0. For the smaller square it is $n(\eta_0) = 3$, for the larger square $n(\eta_0) = 5$. To every saturated spot A_i corresponds a function Ψ_i, which, for a fixed value of ξ_{us}, is constant in time. With enlarging square $[-\eta_0, \eta_0]^2$, more and more spots are included. As the spots are advected by $\mathbf{u}^{(0)}$ (indicated by arrows), the choice of spots located inside any finite square change depends on τ, corresponding to a rearrangement of the series $\sum_{i=1}^{\infty} \Psi_i$. In the limit, however, all spots are included and assuming absolute convergence of the series, every rearrangement converges to the same limit Ψ.*